Eur. Phys. J. A **6**, 309–324 (1999)

THE EUROPEAN PHYSICAL JOURNAL A

Single and double π^o-photoproduction from the deuteron

B. Krusche[1], J. Ahrens[2], R. Beck[2], M. Fuchs[1], S.J. Hall[3], F. Härter[2], J.D. Kellie[3], V. Metag[1], M. Röbig-Landau[1,a], H. Ströher[1,b]

[1] II. Physikalisches Institut, Universität Giessen, 35392 Giessen, Germany
[2] Institut für Kernphysik, Johannes-Gutenberg-Universität Mainz, 55099 Mainz, Germany
[3] Department of Physics and Astronomy, University of Glasgow, Glasgow G128QQ, UK

Received: 24 June 1999 / Revised version: 30 August 1999
Communicated by Th. Walcher

Abstract. Photoproduction of neutral pions from the deuteron has been studied for incident photon energies from 200 MeV to 792 MeV with the TAPS detector at the Mainz MAMI accelerator. Total and differential cross sections covering the full angular range have been obtained for coherent and incoherent single π^o-photoproduction. Good agreement between model predictions and the data was found for the coherent process. The incoherent cross section in the energy region of the $\Delta(1232)$-resonance is overestimated by existing models. A comparison to model predictions indicates that final state interaction effects are much more important than for the coherent reaction. However, the angular dependence of the data in the Δ-peak region follows the pattern expected from the dominant excitation of the M_{1+}-multipole on the free nucleon. The energy and angular dependence of single π^o-photoproduction in the second resonance region is remarkably different from the reaction on the free proton, indicating a strong nuclear effect. Finally the total cross section for double π^o-photoproduction from the deuteron has been measured for the first time and was used to estimate the cross section for double π^o-photoproduction from the neutron.

PACS. 13.60.Le meson production – 25.20.Lj photoproduction reactions

1 Introduction

The study of nucleon resonances is a very important testing ground for modern hadron models. Since the resonances decay dominantly by the emission of mesons to the nucleon ground state photoproduction of mesons is the ideal tool to study the electromagnetic transition amplitudes which are connected to the spin – flavor degrees of freedom of the nucleon. Photoproduction of neutral mesons plays a special role for the study of resonance contributions since background contributions like e.g. meson pole terms or Kroll-Rudermann terms are strongly suppressed due to the weak coupling of the photon to neutral mesons. The photoproduction of pions from the free proton was extensively used to study the properties of the $\Delta(1232)$-resonance as well as resonances at higher excitation energies. Similarly, photoproduction of η-mesons from the proton was very succesful in providing information on the properties of the $S_{11}(1535)$ [1,2] resonance.

Photoproduction from the proton alone tells us nothing about the isospin structure of the electromagnetic transitions. It is thus desirable to investigate the same reactions also on the neutron, but due to the non-availability of neutron targets one must rely on meson photoproduction from light nuclei. In principle there are two possibilities to learn about the isospin structure of the photoexcitation amplitudes. Coherent photoproduction from light nuclei may be used as an isospin filter while photoproduction from bound nucleons in quasifree kinematics can be used to extract the neutron cross section. The small binding energy and the comparatively well understood nuclear structure single out the deuteron as exceptionally important target nucleus. The reactions $d(\gamma,\pi^-)pp$ [3], $d(\gamma,\eta)np$ [4,5] and $d(\gamma,\pi^o\pi^-)pp$ [6] were already used to investigate the respective reactions from the neutron. Furthermore photoproduction from the deuteron bridges the gap from the elementary reaction on the free proton to the photoproduction from heavier nuclei which is of much interest for the study of the behavior of nucleon resonances in the nuclear medium.

Even in the favorable case of the deuteron however, the measured cross sections are influenced by nuclear effects like e.g. the rescattering of the mesons. The extraction of the elementary $n(\gamma,x)n$ amplitudes requires input from models at least for the off-shell behavior of the nucleons and the treatment of final state interactions. For neutral pions predictions were made by several models for the re-

Send offprint requests to: bernd.krusche@exp2.physik.uni-giessen.de

[a] *Present address:* SAP, 69190 Walldorf, Germany
[b] *Present address:* Institut für Kernphysik, Forschungszentrum Jülich GmbH, 52425 Jülich

actions $d(\gamma,\pi^o)d$ (see e.g. [8,9,7,10,11] and ref. therein), $d(\gamma,\pi^o)np$ [8,12,13] and $n(\gamma,\pi^o\pi^o)n$ [14,15].

So far the data basis to test such predictions is very small. Some experiments have investigated coherent π^o-photoproduction from the deuteron in the Δ-resonance region or at higher energies [16–20]. These experiments used untagged Bremsstrahlung beams and most of them identified the reaction by a momentum analysis of the recoil deuterons in a magnetic spectrometer. This technique did not allow the investigation of pions emitted at forward angles since the energy of the corresponding deuterons was too low. Consequently most of the data are concentrated at pion cm angles larger than 60^o. One experiment [16] studied $d(\gamma,\pi^o)d$ at 6^o by an identification of the pions via their two-photon decay without detection of the recoil deuteron. However, in this approach events from the breakup reaction also contributed. The effect was corrected by subtracting from the data an estimate of the breakup reaction obtained from the free proton cross section, which gave rise to systematic uncertainties. Very recently inclusive angular distributions of the $d(\gamma,\pi^o)np$ and $d(\gamma,\pi^o)d$ reactions were measured [21] close to threshold at incident photon energies below 160 MeV where the reaction is expected to be dominated by the coherent process. At higher photon energies in the excitation range of the Δ-resonance no complete angular distributions and hence no total cross sections were reported up to now.

Quasifree single π^o-photoproduction from the deuteron with coincident detection of recoil protons and neutrons was measured with rather large uncertainties from 260–420 MeV [22], 450–800 MeV [23] and 500–900 MeV [24] for angles larger than 45^o with untagged bremsstrahlung. No data has been reported up to now for double π^o-photoproduction from the deuteron.

In the present work, inclusive, coherent and incoherent single and quasifree double π^o-photoproduction from the deuteron have been investigated from the Δ-resonance up to the second resonance region comprising the $P_{11}(1440)$, $D_{13}(1520)$ and $S_{11}(1535)$ resonances. A consistent set of angular distributions for coherent and incoherent single π^o-photoproduction covering the full angular range was obtained. The total cross section of the $d(\gamma,2\pi^o)d$ reaction was measured for the first time and used to estimate the cross section of double π^o-photoproduction from the neutron.

2 Experimental setup

The experiment has been carried out at the Mainz Microtron (MAMI) [25]. The 855 MeV cw electron beam was used to produce quasi-monochromatic photons by means of bremsstrahlung tagging with the Glasgow/Mainz tagged photon facility [26]. Typical beam intensities of 5×10^5 photons MeV^{-1} s^{-1} and an energy resolution of 1-2 MeV were available with the tagging spectrometer for photon energies up to 790 MeV. Data were taken in two separate runs, the first in the energy range from 200–790 MeV and the second covering only energies above 520 MeV. During the second run the high voltage of photomultipliers for tagger counters at lower photon energies was turned off. This allowed an increase of the electron beam intensity which provided the high photon flux also in the high energy range. The collimated beam passed through a 10 cm long, 5 cm diameter liquid deuterium target located approximately 12 m downstream of the radiator. The target container was made entirely from Kapton foil with 60 μm thick entrance and exit windows. The beam spot diameter on the target was approximately 3 cm.

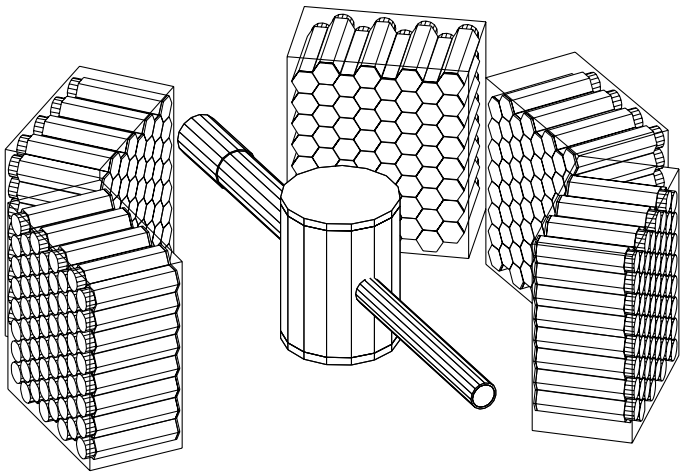

Fig. 1. Setup of the TAPS-detector at the Mainz MAMI accelerator. Five TAPS blocks each consisting of 64 BaF_2 modules arranged in an 8x8 matrix were placed in one plane around the target chamber with the liquid deuterium target. With the exception of the most backward block all BaF_2 modules were equipped with individual plastic veto detectors The beam entered the target chamber from the lower right edge.

Neutral pions produced in the target were detected via their 2γ-decay with the TAPS detector system [27]. The experimental setup is shown in Fig. 1. The spectrometer consists of hexagonally shaped BaF_2-modules of 25 cm length corresponding to 12 radiation lengths. They were equipped with individual plastic veto detectors and 64 modules were arranged in an 8×8 matrix to form one TAPS block. For the experiments discussed here five TAPS blocks with a total of 320 detector modules were available. They were placed in one plane around the target at a distance of 55 cm and at polar angles of $\pm38^o$, $\pm88^o$ and $+133^o$ as indicated in Fig. 1. The block placed at most backward angles was not equipped with veto detectors. The photon response of the spectrometer was investigated by moving one block into the photon beam. Details of the energy calibration and the measured response are given in [28].

3 Data analysis

3.1 Identification of π^o-mesons

In the first step of the analysis particles must be discriminated from photons. Most charged particles were rejected

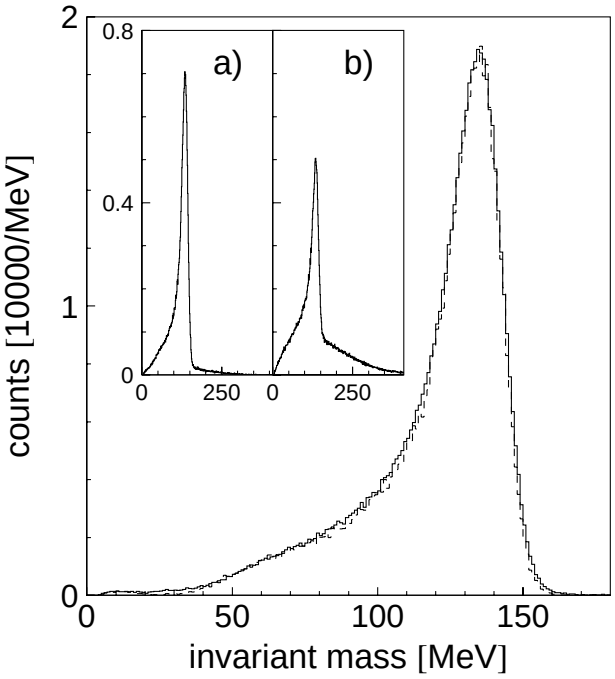

Fig. 2. Measured invariant mass spectra. The main picture shows the invariant mass distribution for incident photon energies between 200–400 MeV. The dashed histogram represents the result of a Monte-Carlo simulation of the detector response. The inserts a) and b) show the measured distributions for incident photon energies between 400–600 MeV and 600–790 MeV, respectively.

with the help of the veto detectors. Neutral particles were identified by time-of-flight and pulse-shape analysis. A time resolution for γ-γ-coincidences in TAPS of 500 ps (FWHM) was achieved. The pulse shape analysis is based on the fact that the scintillation light from BaF_2 crystals is composed of two components with very different decay times. The relative intensity of the fast component is different for photons and particles. This feature was exploited by integrating the signals over a short gate period (50 ns) and a long gate period (2μs). Since the pulse shape discrimination works best for high energies while the time-of-flight method is most effective for low energies, the combination of both very effectively separates photons from recoil particles.

Neutral pions were identified with a standard invariant mass analysis using

$$M_{inv} = (2E_{\gamma 1}E_{\gamma 2}(1 - cos(\Phi_{\gamma\gamma}))^{1/2}, \qquad (1)$$

where $E_{\gamma 1}$, $E_{\gamma 2}$ are the photon energies and $\Phi_{\gamma\gamma}$ is the opening angle between them. Typical invariant mass spectra are shown in Fig. 2. A resolution of ≈23 MeV FWHM was achieved. The tail of the peak at the low energy side stems mainly from shower losses at the back of the BaF_2-modules. The spectrum is practically free of background at incident photon energies below ≈ 400 MeV which demonstrates the excellent particle suppression. Also shown in the figure is the result of a Monte Carlo simulation of the detector response with the GEANT code [29] (see Sect. 3.3) which matches the measured distribution very well. The combinatorial background visible for higher incident photon energies originates from double π^o-production and η-decays into three neutral pions. This background is removed for single and double π^o production by cuts on missing energy or missing mass (see below). Inclusive π^o-production was analysed by subtracting the fitted combinatorial background separately for each bin of incident photon energy and pion polar angle. The background from random coincidences between TAPS and the tagging spectrometer was determined by shifting the time-of-flight cut away from the prompt peak and subsequently subtracted.

3.2 Identification of reaction channels

At incident photon energies below 309 MeV only the reactions $d(\gamma,\pi^o)d$, $d(\gamma,\pi^o)np$ and $d(\gamma,\pi^o\gamma)X$ can contribute to the production of neutral pions. Since the $\pi^o\gamma$ final state has a negligible cross section only coherent and incoherent single π^o-production are of importance. Recoil deuterons were not detected in the present experiment. Coherent and incoherent contributions were separated by their different reaction kinematics.

This was done by generating missing energy spectra from a comparison of the kinetic cm energy of the pion derived from the measurement of energy and momentum of its decay photons $E^\star_m(\gamma_1\gamma_2)$ to the kinetic energy derived from the incident photon energy $E^\star_m(E_\gamma)$ under the assumption of pion production on a *deuteron*:

$$\Delta E_m = E^\star_m(\gamma_1\gamma_2) - E^\star_m(E_\gamma). \qquad (2)$$

It is evident from Fig. 3 that the experimental resolution was not good enough for an event-by-event separation of the two reaction types. However, their contributions could be extracted from a comparison of the data to the simulated response for the coherent reaction and the breakup reaction. The peak for the quasifree reaction is shifted away from zero and broadened by the Fermi motion of the nucleons which was taken into acount for the simulation in a participant – spectator model. The separation is quite good at backward angles but less so at forward angles so that the forward cross section data is subject to larger systematic uncertainties.

At higher energies the cross section for coherent π^o-production is negligible compared to the breakup reaction, but additionally π^o-mesons are produced by the double pion production reactions $d(\gamma,\pi^o\pi^+)nn$, $d(\gamma,\pi^o\pi^-)pp$ and $d(\gamma,\pi^o\pi^o)np$. The contribution from triple pion production is negligible below the η-production threshold (E_{thr} ≈ 628 MeV) but at higher energies the η-decay channels $\eta \to 3\pi^o$ and $\eta \to \pi^o\pi^+\pi^-$ contribute in addition.

The experimental resolution was good enough for an event-by-event separation of single π^o-production from multiple pion production reactions again based on a miss-

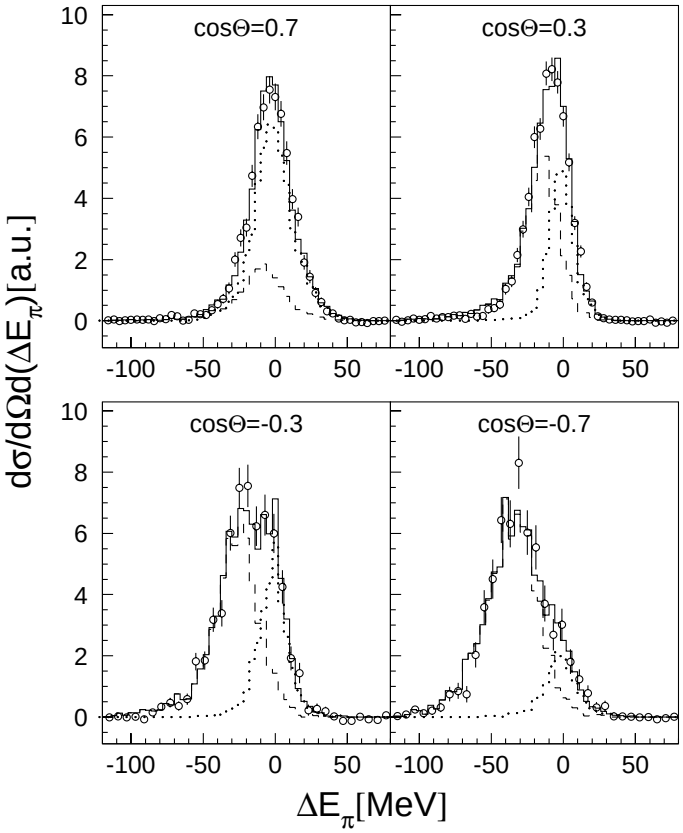

Fig. 3. Missing energy spectra for the separation of the reactions $d(\gamma,\pi^o)d$ and $d(\gamma,\pi^o)np$ at an incident photon energy of 290 MeV for four different π^o cm-angles. The dashed (dotted) histograms represent the simulation of the quasifree (coherent) reaction. The full histograms the sum of both which is compared to the data.

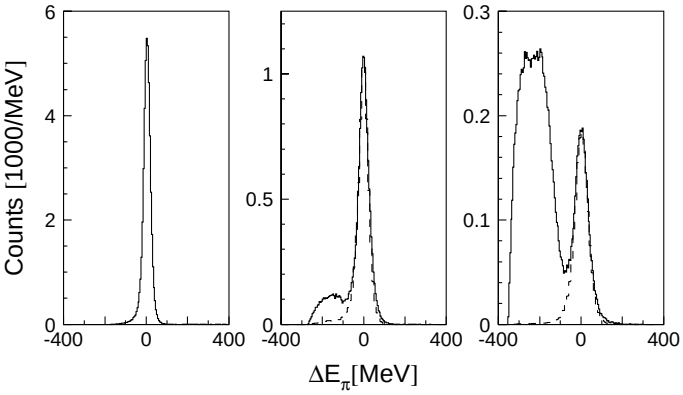

Fig. 4. Missing energy spectra for the reaction $d(\gamma,\pi^o)np$. The full histograms represent the measured data. The dashed histograms are the result of a Monte-Carlo simulation that includes effects of Fermi smearing for the bound nucleons and the response of the detector system. The spectra from left to right correspond to incident photon energy ranges of 280–400 MeV, 400–600 MeV and 600–790 MeV, respectively. The background in the medium and high energy range stems from multiple pion production.

ing energy analysis of the reaction kinematics. In this case the missing energy was determined assuming pion production on a free nucleon at rest. The missing energy peaks for the breakup reaction $d(\gamma,\pi^o)np$ are of course broadened by Fermi motion of the bound nucleons and the component from coherent production is slightly shifted due to the different recoil mass. However as shown in Fig. 4 the superposition of both is clearly separated from the events due to multiple pion production. The result of a Monte Carlo simulation of the $d(\gamma,\pi^o)np$ reaction taking into account the detector response and the effects of nuclear Fermi motion is compared to the data in Fig. 4. The single pion production peak is very well reproduced for incident photon energies above $\approx$ 400 MeV where contributions from the coherent reaction are negligible. At lower energies the analysis described above was used to separate coherent and incoherent events.

Events from the reaction $d(\gamma,\pi^o\pi^o)np$ were identified as described in detail elsewhere [30] for the reaction on the free proton. At photon energies below the η-threshold the cross section was obtained in two different ways. In the first analysis all events with three identified photons were taken. This analysis relies on the facts that no other reaction with more than two photons in the final state contributes significantly and that contaminations from misidentified particles and scattered photons are negligible. The first condition is fulfilled due to the very small cross sections of reactions like $d(\gamma,\pi^o\gamma)np$ and triple pion production with at least two neutral pions. Particles were very efficiently removed from the data sample with the methods discussed in 3.1. False photon pairs which result from the split-off of an electromagnetic shower into two geometrically unrelated components were eliminated with cuts on the relative photon timing, the minimum photon energy and the minimum opening angle between photons.

In the second analysis only events with four photons which could be combined in a unique way into two photon pairs each with the invariant mass of a π^o-meson were included. If the effects of nuclear Fermi motion are ignored such events are kinematically overdetermined which allows the calculation of the mass of the missing recoil nucleon m_N from the photon beam energy E_b and momentum $\boldsymbol{P_b}$ and the energies E_{γ_i} and momenta $\boldsymbol{P_{\gamma_i}}$ of the four decay photons. Nuclear Fermi motion causes only a slight broadening of the missing mass peak. The overdetermination was used for a missing mass analysis based on:

$$\Delta M = m_N - \sqrt{(E_b + m_N - \sum_{i=1}^{3} E_{\gamma_i})^2 - (\boldsymbol{P_b} - \sum_{i=1}^{3} \boldsymbol{P_{\gamma_i}})^2}. \quad (3)$$

The result of the analysis is shown in Fig. 5. The missing mass spectrum is practically free of background at incident photon energies below the η-threshold. The background structure at higher photon energies is due to the decay of the η-meson into three neutral pions.

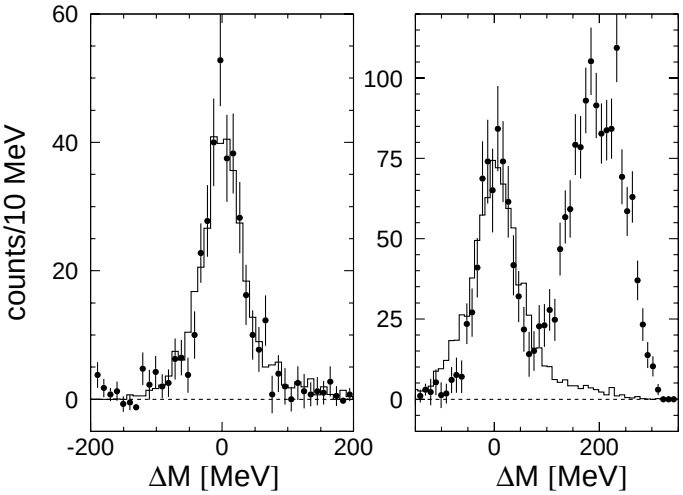

Fig. 5. Missing mass spectra for the reaction $d(\gamma,\pi^o\pi^o)np$. The left hand side corresponds to incident photon energies below the η-threshold, the right hand side to energies above the η-threshold. The symbols show the measured data, the histograms are the results of a Monte-Carlo simulation including Fermi smearing of the bound nucleons and the response of the detector system.

3.3 Determination of cross sections

The absolute cross sections were obtained from the number of events, the thickness of the liquid deuterium target ($1.73\ g/cm^2$), the intensity of the photon beam and the detection efficiency of TAPS. The photon intensity was determined by counting the deflected electrons in the tagging spectrometer and measuring the tagging efficiency (i.e. the fraction of the correlated photons which pass through the photon collimator) by reducing the intensity and moving a lead glass detector into the photon beam (approximately twice a day).

The angle and energy dependent detection efficiency of TAPS was modelled with Monte Carlo simulations, carried out with the GEANT3 code [29]. The detection efficiency for single pion production was simulated as a function of laboratory angle and kinetic energy of the pions and corrected event-by-event. In this way the correction is independent of any assumptions about the reaction kinematics which e.g. in case of the breakup reaction are not trivial. Only at energies above 300 MeV a correction depending on reaction kinematics had to be applied for the extreme forward and backward angles (10^o, 170^o) which accounted for a zero acceptance region in the Θ_π-E_π-plane. Apart from this correction model dependent simulations were only used for the separation of the coherent and incoherent single pion data. The excellent agreement of the simulations with the data is demonstrated in Figs. 2–4.

The detection efficiency for $2\pi^o$-photoproduction was simulated taking into account the Fermi motion of the bound nucleons derived from the deuteron wave function [33] and assuming phase space distribution of the two pions. This assumption is well justified since it has been shown for the elementary reaction on the proton [30] that the $\pi^o - \pi^o$ invariant mass exhibits phase space behavior (which is not true for the π^o-p invariant mass). The good description of the reaction kinematics for 4-photon events is demonstrated in Fig. 5. An additional check of this efficiency simulation comes from the fact that the results obtained for the total cross section from an analysis of three and four photon events (with detection efficiencies different by more than an order of magnitude) are in very good agreement. Nevertheless, the systematic uncertainty is larger than for the completely model independent detection efficiency of the single pion data.

The following systematic uncertainites of the overall normalization must be taken into account: analysis cuts on time-of-flight, pulse shape etc. (2%), target thickness (2%), photon flux (1%) and Monte Carlo simulation of detection efficiency (5% for single π^o data, 10% for $2\pi^o$). Consequently the overall systematic uncertainty is roughly 6% for single and 10% for double π^o data. It should be noted that the comparison of cross sections measured from the deuteron to those from the proton has a much smaller relative systematic uncertainty since both data sets were measured with the same setup and most uncertainties effect them in the same way.

4 Results and discussion

4.1 Inclusive single π^o-photoproduction

The total and differential cross section for inclusive single π^o-photoproduction from the deuteron normalized to the mass number are compared to the data from the proton in Figs. 6–8. The low energy proton data from production threshold to 280 MeV are taken from [31], the data up to 650 MeV from [32] and the high energy data up to 790 MeV are from the present work. It should be noted that all data sets have been measured with the same setup in three consecutive runs optimized for the different incident photon energy ranges. The angular distributions in Fig. 7 are given in the cm system of the incident photon and a nucleon at rest. This facilitates a direct comparison of the breakup process, which dominates the reaction at higher energies, to the elementary reaction on the proton. Throughout this paper cross sections in the photon – nucleon cm are labelled (*N), while cross sections in the photon – deuteron system, which is more appropriate for the discussion of coherent photoproduction are labelled (*d). The incoherent differential cross sections have been fitted with the simple ansatz:

$$\frac{d\sigma}{d\Omega} = \frac{q_\pi^*}{k_\gamma^*}[a + b \times cos(\Theta_\pi^{*N}) + c \times cos^2(\Theta_\pi^{*N})] \quad (4)$$

where q_π^* and k_γ^* are the pion and photon cm momentum, respectively. The fits are compared to the data in Fig. 7.

We discuss this data for three different energy regions: the peak region of the Δ-resonance, the intermediate energy range between 400 and 650 MeV and the so-called second resonance region above 700 MeV.

The total cross section per nucleon in the Δ-peak shows a remarkable reduction compared to the reaction

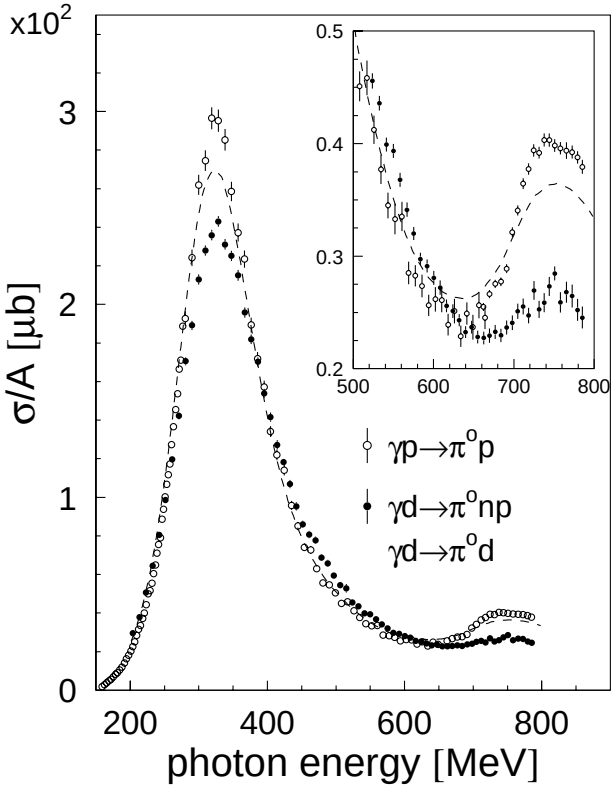

Fig. 6. Comparison of the total cross section for single π^o-photoproduction from the deuteron and the proton normalized to the mass number. Open symbols: cross section of $p(\gamma,\pi^o)p$, full symbols: sum of the cross sections of $d(\gamma,\pi^o)np$ and $d(\gamma,\pi^o)d$. The dashed line corresponds to the proton cross section folded with the Fermi motion of nucleons bound in the deuteron. The insert is a magnification of the second resonance region.

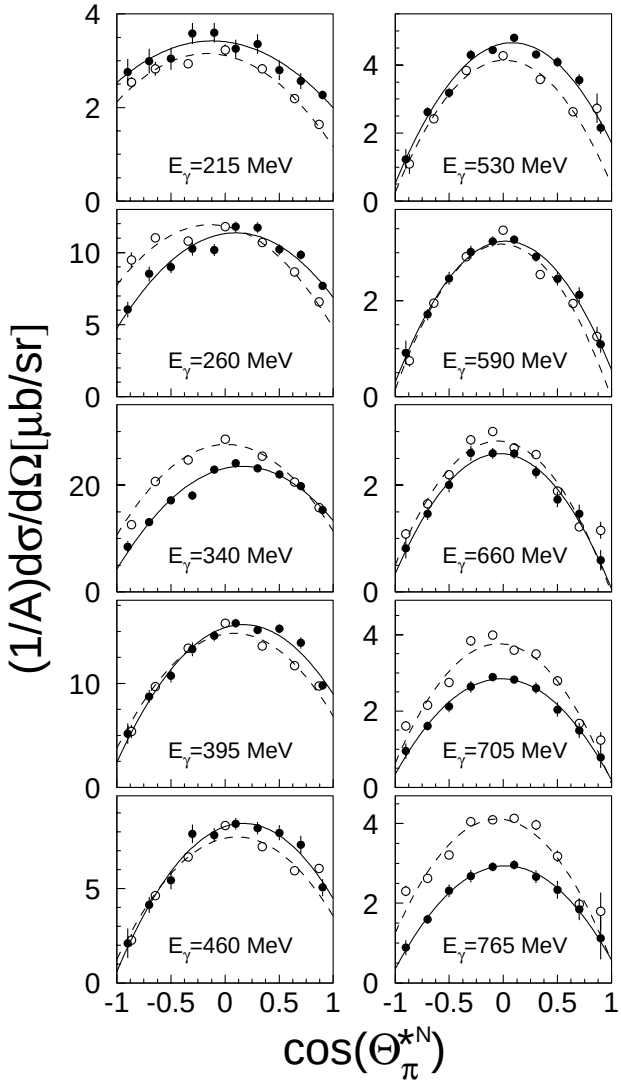

Fig. 7. Differential cross sections for single π^o-photoproduction from the deuteron (filled circles) and the proton (open circles). The full curves are the results of fits to the deuteron data and the dashed curves represent the fits of the proton data (see text).

on the free proton (see Fig. 6). An earlier measurement of the ratio

$$R = \frac{d\sigma}{d\Omega}[\gamma d \to \pi^o n] / \frac{d\sigma}{d\Omega}[\gamma d \to \pi^o p] \qquad (5)$$

at backward angles ($> 90^o$) [22] found a value close to unity and the reduction cannot be explained alone by smearing of the cross section due to Fermi motion of the bound nucleons. This is demonstrated in Fig. 6 by a comparison to the proton cross section folded with the momentum distribution of the bound nucleons which was calculated from the deuteron wave function [33]. A similar effect is observed in the total photoabsorption cross sections on the proton and deuteron [34,35], where the peak cross section per nucleon from the deuteron is about 70 μb lower than the free proton cross section. Since the difference in peak cross sections for single π^o-photoproduction found here amounts to about 55 μb this explains most of the effect seen in total photoabsorption and consequently the behavior of neutral pion production from the deuteron must be very different from the charged channels. We will come back to this point in the discussion of the breakup reaction. The angular distributions on the proton and deuteron (see Fig. 7) are somewhat different in this angular range, which is not unexpected since the deuteron data is a superposition of coherent and incoherent processes.

The total and differential cross sections in the intermediate energy range above 400 MeV where coherent π^o-photoproduction becomes negligible are quite similar for the proton and the deuteron, although around 550 MeV the cross section per nucleon from the deuteron is somewhat larger than the proton cross section. In two previous experiments Bacci et al. [23] and Hemmi et al. [24] measured the R ratio defined above for angles between 60^o and 140^o and found values between 1.5 and 2 in the energy range from 500–600 MeV incident photon energy. They took this result as evidence for a large isoscalar part

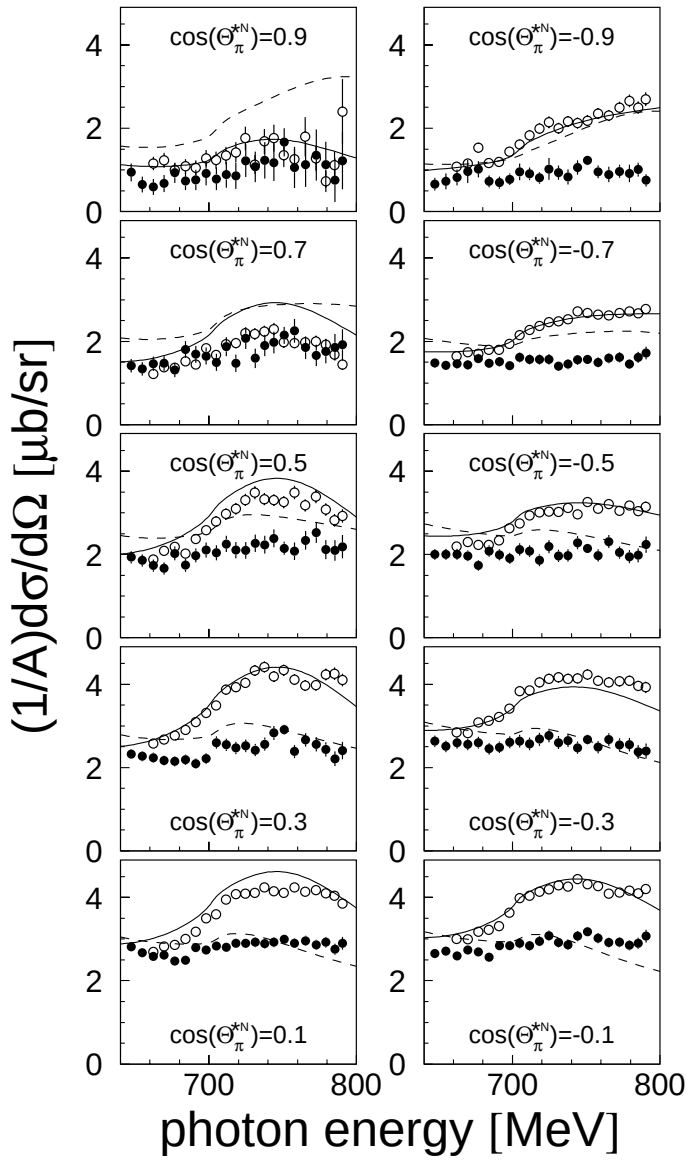

Fig. 8. Comparison of the differential cross sections for the reactions $d(\gamma,\pi^o)np$ (filled circles) and $p(\gamma,\pi^o)p$ (open circles) in the second resonance region. Shown are the differential cross sections as function of incident photon energies for 10 different values of the cosin of the cm polar angle. The full curves represent the result of the multipole analysis from the SAID program for $p(\gamma,\pi^o)p$ and the dashed curves the same results for $n(\gamma,\pi^o)n$.

in the photoexcitation of the $P_{11}(1440)$ resonance. The inclusive cross section per nucleon from the present experiment for backward angles (see Fig. 7) comes very close to the proton data. These results are not neccessarily in contradiction since off-shell effects and final state interaction effects, which are expected to cancel to a large extent in the ratio, could by chance produce the agreement of the inclusive cross section per nucleon at backward angles with the proton cross section. However, Bacci et al. themselves report correction factors for the deuteron effects obtained from a comparison of π^o-photoproduction from the free proton and the bound proton that are not large enough to account for the discrepancy.

The proton cross section shows a pronounced structure at the highest incident photon energies which is almost completely suppressed on the deuteron (see Figs. 6, 7,8). Bacci et al. [23] report R values close to unity for this energy range and correction factors for the deuteron effects of just a few per cent. This is in contradiction with the present data. In their experiment π^o-mesons were identified by the detection of one decay photon with lead glass detectors. No kinematical reconstruction was possible. Consequently, the experiment relied on the assumption that contributions from multiple pion production can be safely neglected. However, in the present experiment we find that at incident photon energies above 600 MeV the cross section is *dominated* by the multiple pion channels. Hemmi et al. [24] measured both π^o-decay photons in coincidence with the recoil nucleon and identified the reaction by kinematical reconstruction. They also report R values close to unity. However, their differential cross sections for π^o-production from the bound neutron and proton are flatter in this energy range than the distributions for the free proton. Although their uncertainites are quite large, this might indicate that the disappearing of the structure is a deuteron effect.

The vanishing of the structure in the $d(\gamma,\pi^o)np$ reaction certainly cannot be explained by nuclear Fermi motion. The proton cross section folded with the nucleon momentum distribution still shows a pronounced peak around 750 MeV (see Fig. 6). For a more detailed discussion differential cross sections for the proton and deuteron data are compared for some angular bins in Fig. 8. With the exception of the extreme forward angles the differential cross sections exhibit the structure in the proton data and an almost energy independent behavior of the deuteron cross section. Also shown in Fig. 8 are the results of the SAID [36] multipole analysis for the $p(\gamma,\pi^o)p$ and $n(\gamma,\pi^o)n$ reactions from the world data base. It is evident that a momentum folded superposition of the two curves cannot explain the deuteron data, in particular not for backward angles. This behavior is in sharp contrast to the findings for η-photoproduction [4,5] and $\pi^+\pi^-$ double pion production [6] where in the same energy range no deuteron effects beyond Fermi motion were observed.

Any interpretation of the different behavior of the proton and deuteron cross section requires an understanding of what causes the structure observed in the proton data in the first place. The rise between 700 and 750 MeV is certainly not only due to the excitation of the $D_{13}(1520)$-resonance. It is known [37] that at least for the backward angles the opening of the η-photoproduction threshold causes a unitarity cusp that results in a pronounced s-shape like step of the cross section around the threshold at 705 MeV. A quantitative analysis of the cusp effect requires a simultaneous multipole analysis of the pion- and η-photoproduction data. Such an analysis is presently under way [38]. The precise data for $p(\gamma,\pi^o)p$ reported here, which were measured simultaneously with the η-photo-

production data reported in [1], will allow a comparison of the two reactions with very small systematic uncertainties.

4.2 Coherent and incoherent π^o-photoproduction

A detailed investigation of single π^o-photoproduction in the Δ-resonance region requires a separation of the coherent and incoherent parts. This was done with the methods discussed in section 3.2. The uncertainties of the data are dominated by the systematic error of the separation procedure. The result for the total cross sections is compared to model predictions in Fig. 9. The predictions for the coherent cross section, in particular from Kamalov et al. [10] and Laget [8], are in good agreement with the data.

4.2.1 Incoherent π^o-photoproduction

The breakup reaction is overestimated by all model predictions (see Fig. 9). Calculations by Schmidt et al. [12] and Laget [8], which do not include final state interaction effects (FSI) overestimate even the measured total inclusive cross section. The prediction by Laget [8] including neutron-proton (np) final state interaction effects is much closer to the data but still too high.

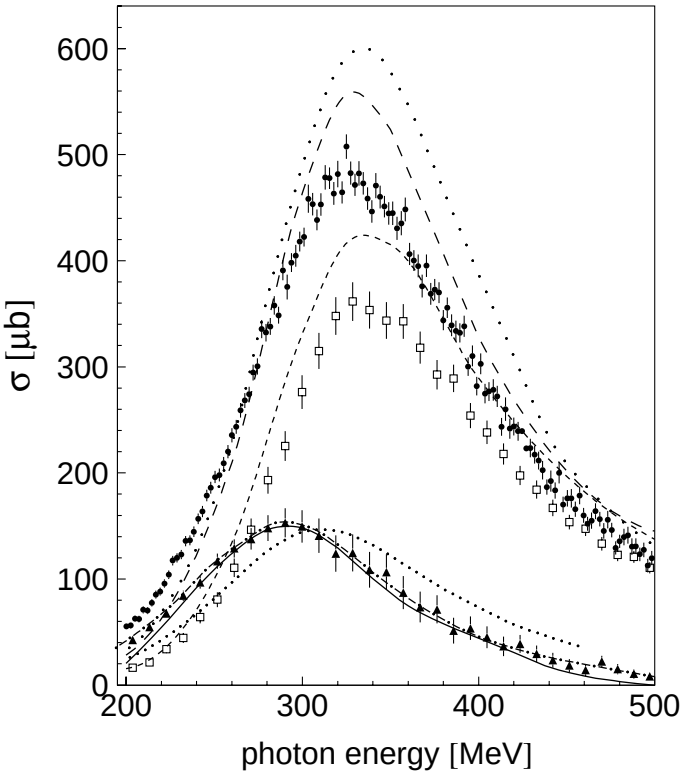

Fig. 9. Total single π^o-photoproduction cross section in the $\Delta(1232)$-resonance region compared to predictions. Filled circles: inclusive single π^o-production, filled triangles: coherent π^o-production, open squares: breakup reaction. Full, dash-dotted and dotted curves: predictions from Laget [8], Kamalov et al. [10] and Wilhelm et al. [11] for coherent production. Long dotted curve: breakup π^o-production from Schmidt et al. [12]. Long dashed (short dashed) curves: breakup production from Laget [8] without (with) np-FSI.

Laget noted already in [8] that even though his calculations reproduced the charged channels and coherent π^o-production quite well, the sum of the cross section from all channels is larger than the measured total photoabsorption cross section [34] in the Δ-peak. He suggested that the total photoaborption data could suffer from systematic effects. However, in the meantime the photoabsorption data was remeasured [35] with exactly the same result. Our present data suggest that a large part of the discrepancy comes from the π^o-breakup channel.

The differential cross sections for the breakup channel in the Δ-resonance region are shown in Fig. 10. The comparison to the participant – spectator calculation by Schmidt et al. [12] and the calculations with and without np-FSI by Laget [8] clearly demonstrate the importance of FSI effects for this channel. On the other hand, the good agreement between data and simulation for the missing energy distributions (see Figs. 3, 4) indicates that for the pion energy distribution nuclear effects beyond Fermi smearing are not important within the experimental resolution.

The extraction of neutron cross sections from such data requires a careful treatment of the FSI effects. Recently, Levchuk et al. [13] studied quasifree π^o-photoproduction from the neutron via the $d(\gamma,\pi^o)np$ reaction in a model that includes pole and loop diagrams and $n-p$- and $\pi-N$-rescattering. They wanted to explore the possibility of measuring the E_{1+}/M_{1+} ratio via photoproduction from the quasifree neutron. The isospin I=3/2 component of this ratio characterizes the relative strength of the recently much discussed (see e.g. [39,40]) quadrupole $E2$-excitation of the Δ-resonance. The idea was that the $n(\gamma,\pi^o)n$ reaction would be very useful for the isosospin separation of the multipoles. In agreement with the results from the Laget model [8] Levchuk et al. find that the largest effects disturbing the extraction of the multipoles for quasifree neutrons arise from the np final state interaction. They predict that these effects lead to a strong reduction of the cross section at pion forward angles, but are much less important for backward angles since the relative energy of the np-pair rises with the pion angle. Our data for the $d(\gamma,\pi^o)np$ reaction qualitatively support this prediction since the disagreement with the participant – spectator approach (see Fig. 11) is most severe at pion forward angles but less pronounced at backward angles. However, a comparison of the data to the Laget model including np-FSI shows some unexplained reduction of the cross section at backward angles. Levchuk et al. point out, that a clean analysis of the $n(\gamma,\pi^o)n$ reaction requires a careful choice of the kinematic conditions enhancing the contribution from quasifree neutrons by cuts on the neutron or proton recoil energy. In the present experiment recoil nucleons were not detected and therefore no direct comparison of the data to their predictions is possible. It

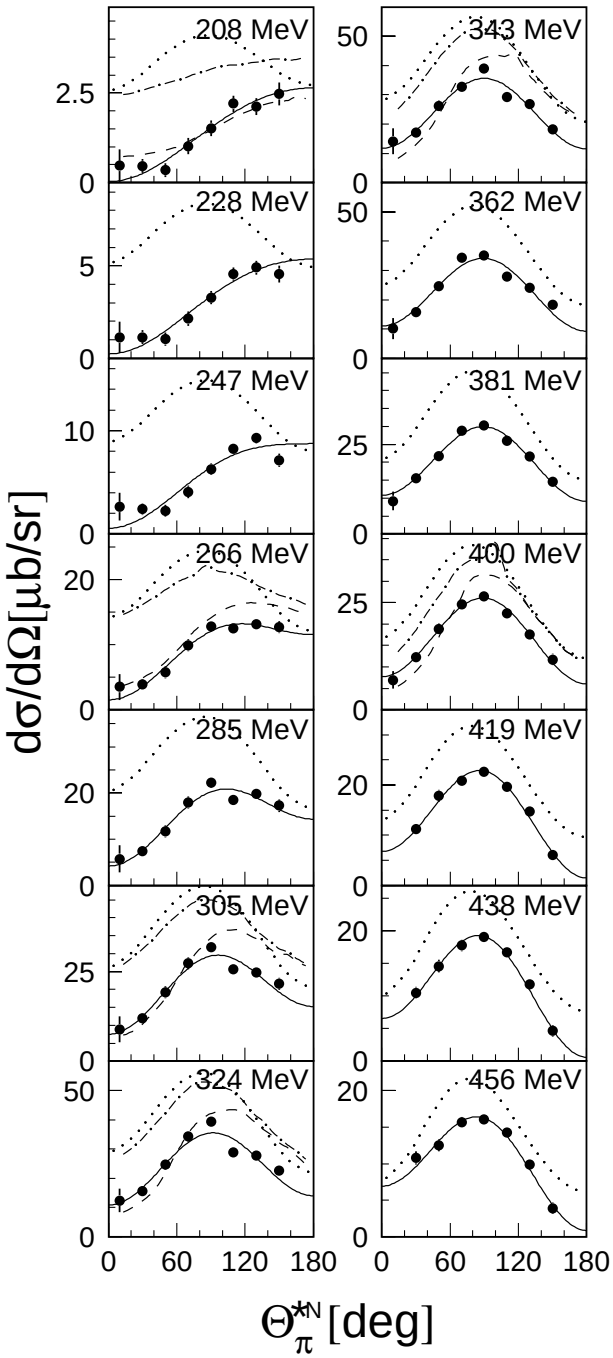

Fig. 10. Differential cross sections for the incoherent $d(\gamma,\pi^o)np$ reaction in the photon-nucleon cm frame. The full curves are fits to the data using (4). The dotted curves show the results of an impulse approximation in the participant – spectator approach from [12]. The dash-dotted (dashed curves) are the results from [8] without (with) np-FSI. These curves were interpolated from photon energies of 200, 260, 300, 325, 350 and 400 MeV.

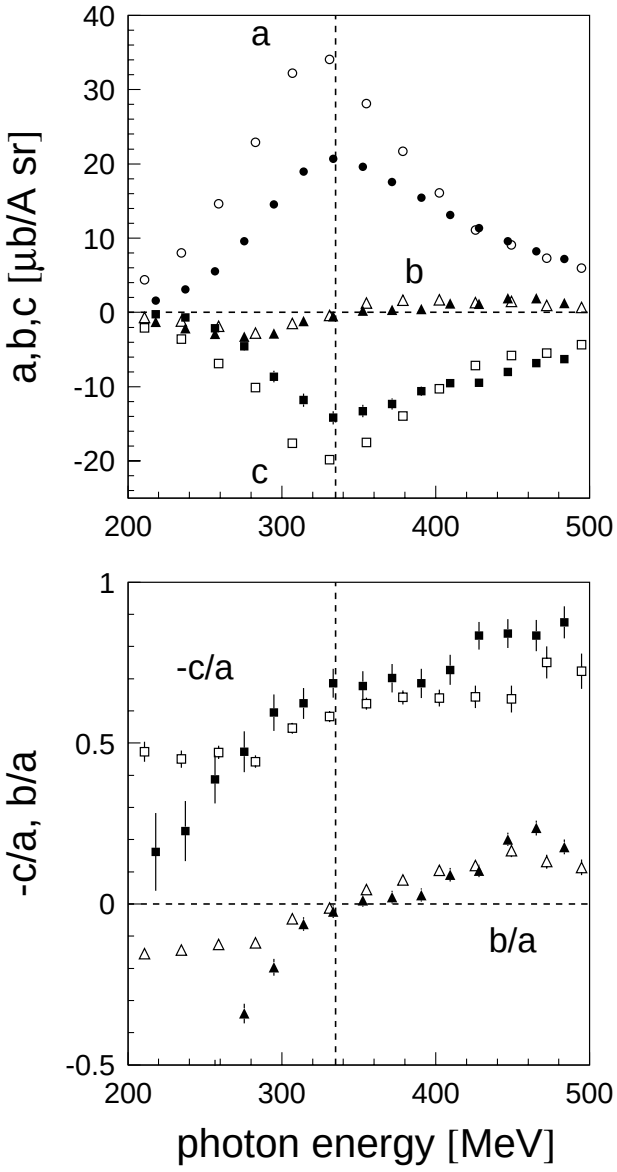

Fig. 11. Fitted coefficients a, b, c of the angular distributions (4) normalized to the mass number (see text) for single π^o-photoproduction from the deuteron (filled symbols, a: circles, b: triangles, c: squares) compared to the proton (open symbols).

is interesting to remark that in spite of the influence of the FSI effects the shape of the angular distributions in the Δ-peak discussed below already exhibits the characteristic features of the Δ-excitation via the M_{1+}-multipole. Future experiments with coincident detection of the recoil nucleons are therefore very promising for an investigation of quasifree π^o-photoproduction from the neutron.

The angular distributions have been fitted with the ansatz from (4) and the results for the coefficients a, b, c are compared in Fig. 11 to the proton data.

Although in the low energy range the angular distributions are quite different from the reaction on the free proton and the absolute values of the differential cross sections are much reduced, their shape close to the resonance position reflects the expected behavior for the quasifree excitation of the Δ-resonance via the M_{1+}-multipole. The resonance position itself is the same for both data sets.

Since the angular distribution of the M_{1+}-multipole is given by

$$\frac{d\sigma}{d\Omega} = \frac{1}{2}\frac{q^*_\pi}{k^*_\gamma}|M_{1+}|^2[5 - 3cos^2(\Theta^{*N}_\pi)], \qquad (6)$$

we expect a ratio c/a = -3/5 as long as all other multipoles can be neglected. The experimental value for quasifree π^o-photoproduction from the deuteron of c/a = -(0.68±0.04) comes very close to this ratio. If we take only s- and p-waves into account, the b-coefficient comes from the interference term:

$$b = 2Re[E^*_{0+}(M_{1+} - M_{1-} + 3E_{1+})]. \qquad (7)$$

Due to the dominance of the M_{1+} the $cos(\Theta^{*N}_\pi)$-term arises from the interference with the E_{0+} which is not resonant and has a negligible imaginary part. The b-coefficient therefore reflects the zero crossing of the real part of the M_{1+}-multipole at the Δ-resonance position.

4.2.2 Coherent π^o-photoproduction

The results for coherent π^o-photoproduction from the deuteron are summarized in Figs. 12,13. The differential cross sections are compared to the earlier results from [16–19]. In general the agreement is reasonable but at 110^o the data from [17] are systematically lower, the lowest energy results from [16] are higher than the present data and the low energy results from [18] are also lower than the present data. It should be noted that all the previous experiments measured cross sections only for selected angular ranges mostly with different spectrometer settings for the different bins and are not always consistent with each other. The present experiment covers the full angular range in the Δ-resonance region with one consistent data set.

The influence of rescattering effects on the coherent π^o-photoproduction from the deuteron, was much discussed in the literature ([7,9,8,10,11]). Bosted and Laget [9,8] investigated the influences of Fermi motion, the deuteron wave function and rescattering effects on the cross section. Their results with and without FSI effects are compared to the data for an incident photon energy of 343 MeV in Fig. 12. Their result from the full calculation is also shown for some other photon energies in Fig. 12. Blaazer et al. [7] studied rescattering corrections to all orders by solving the Faddeev equations of the πNN-system. An example of their results for an incident photon energy of 300 MeV is compared to the data in Fig. 12. Kamalov et al. [10] have studied coherent π^o-photoproduction from the deuteron in a coupled channel approach, treating final state interactions in multiple scattering theory. They argue that the main mechanism of final state interaction in the Δ-resonance region is elastic pion scattering while the contribution from charge exchange reactions, which is very important in the threshold region (see [21]), becomes very small.

On the other hand, Wilhelm et al. [11] treated the rescattering in a more microscopic dynamical model for

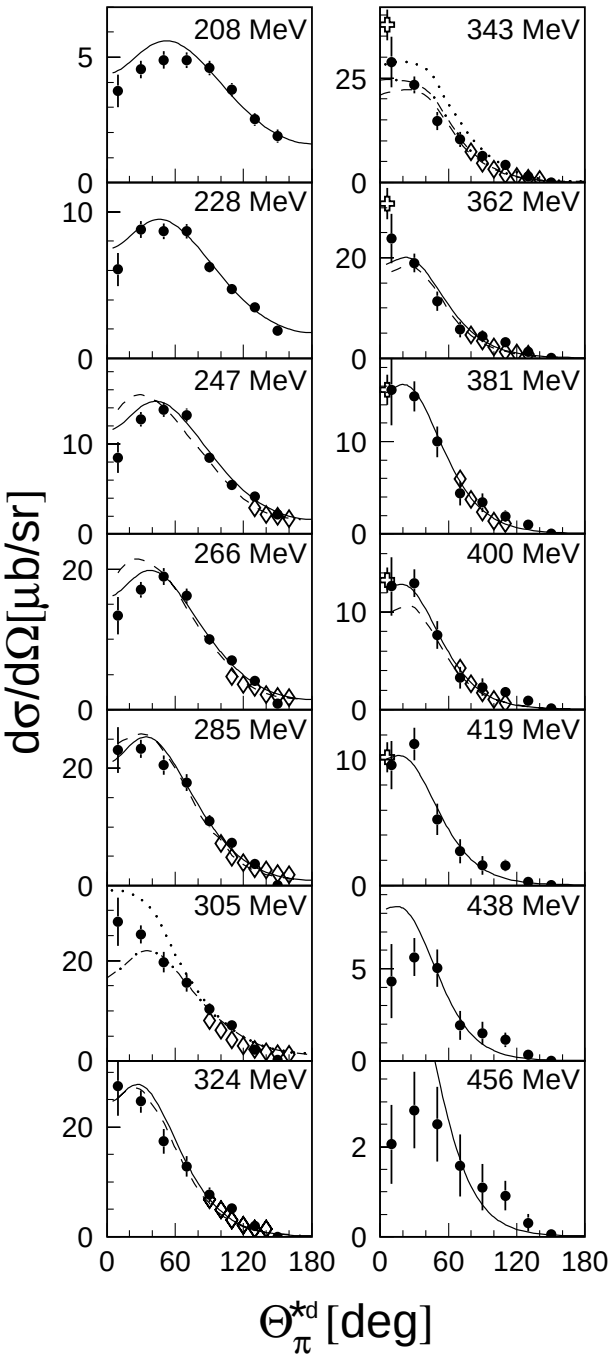

Fig. 12. Angular distributions for the reaction $d(\gamma,\pi^o)d$ in the photon – deuteron cm frame. Filled circles: present experiment, open diamonds: [17], open crosses: [16]. The curves for E_γ=305 MeV are from [7] (dotted: no FSI, dashed-dotted, full: full calculation), the curves for E_γ=343 MeV are from [9] (dotted: s-wave without Fermi motion, dash-dotted: s- and d-waves with Fermi motion, dashed: with rescattering). For all other energies solid curves are from ref [10] and dashed curves from [8].

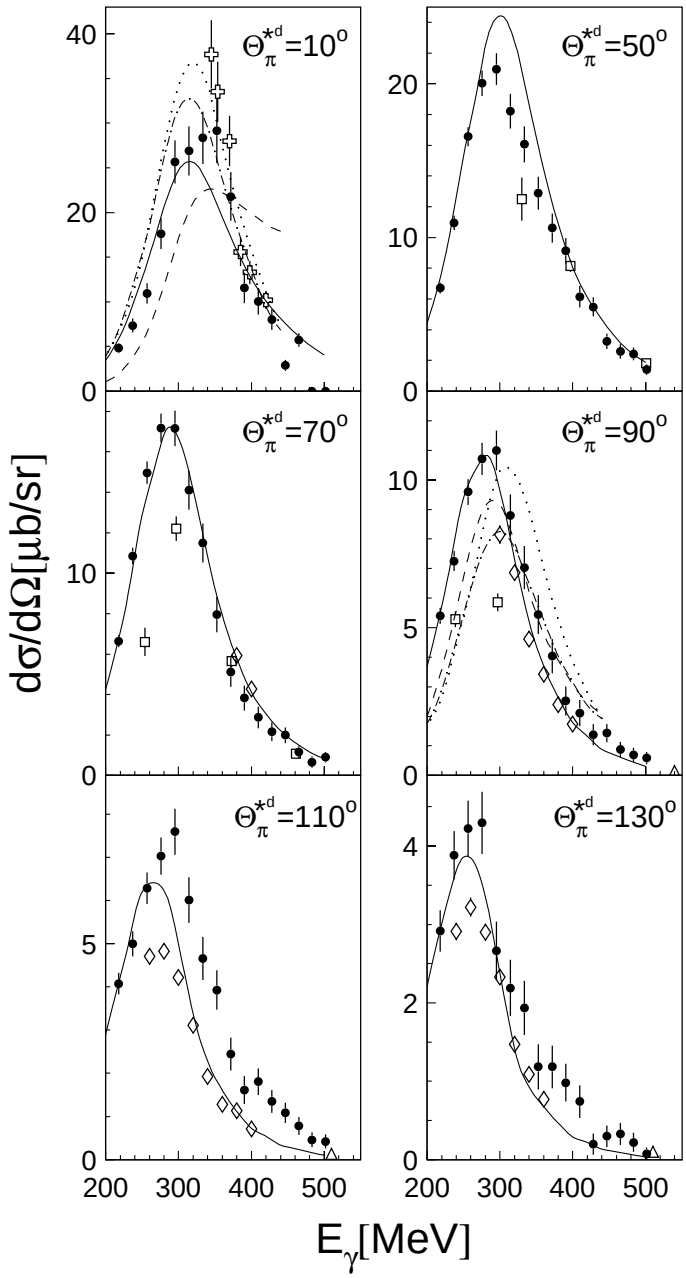

Fig. 13. Differential cross sections for the $d(\gamma,\pi^o)d$ reaction in the photon – deuteron cm frame as function of the incident photon energy. Symbols for data as in Fig. 12, in addition: open squares: [18], open triangles: [19]. The solid and dash-dotted curves show the predictions from [10,11] for the full calculation and the dashed and dotted curves the results from [10,11] without FSI effects, respectively.

the coupled $N\Delta$-, $NN\pi$-and NN-systems and found appreciable contributions from charge exchange amplitudes. Predictions from these two models are compared to the data in Figs. 9, 12, 13. The influence of FSI effects is very different in the models.

In general the agreement between data and model predictions is good but less so for the more ambitious dynamical model of [11]. The comparison of all models to the data suggests the presence of some rescattering effects, but so far no common conclusion about their importance is possible since the various models disagree even qualitatively. Some models predict a reduction of the cross section due to FSI where others predict an increase (see Fig. 13). However, it is evident that FSI effects are less important for the coherent channel than for the breakup channel.

Unfortunately the effects in the models are most pronounced at the extreme forward angles where the uncertainty of the data from the coherent – incoherent separation is largest. However, the present data improves the situation significantly since at the lower photon energies no data at all for the test of the models was available and in the Δ-resonance region all models were conflicting with the 6^o cross sections reported in [16].

4.3 Double π^o-photoproduction

Among the double pion photoproduction reactions on the proton in the second resonance region only double π^o-photoproduction is known to be dominated by the excitation of a N^* resonance and its subsequent sequential decay via an intermediate $\Delta\pi$-state. This was demonstrated by the Dalitz-plot analysis of an earlier experiment with TAPS at MAMI [30]. The photocoupling and the decay branching ratio into $\Delta\pi$ of the $D_{13}(1520)$) resonance are larger than for the neighboring $P_{11}(1440)$ and $S_{11}(1520)$ resonances [45]. Thus the contribution of the D_{13}-resonance is the probably most important one.

Double charged pion production from the proton involves mainly the excitation of the Δ-resonance via the Δ-Kroll-Rudermann (KR) and the Δ pion-pole term. The contribution of N^* resonance excitation alone is small. Only the interference between the sequential decay of the D_{13} resonance and the Δ-KR term is important [14, 42]. The reaction mechanism for the $\pi^0\pi^+$-reaction is still not understood [41,6,14,42]. Double π^o-production thus seems to offer the cleanest tool for the study of the $D_{13}(1520)$ resonance.

This is in particular of interest for the excitation of nucleon resonances in the nuclear medium. The complete suppression of the so-called second resonance bump observed in total photoabsorption experiments with nuclear targets [43] has motivated exclusive experiments in this energy region. In a study of η-photoproduction [44], which is strongly dominated by the S_{11}-resonance no unexplained depletion of the in-medium strength was observed. However, the total contribution of the $S_{11}(1535)$ to the second resonance bump is small and the interpretation of the resonance itself is unclear [46,47]. Double pion production is much more important in this energy range and double π^o-photoproduction can be used for a similar study of the in-medium properties of the D_{13}. In particular a comparison of double π^o- and $\pi^+\pi^-$-production can discern whether medium modifications of the D_{13} (e.g. collision broadening) or a disturbance of the interference between N^*-excitation and Δ-KR term in the nuclear medium [48] is responsible for the suppresion of the resonance bump.

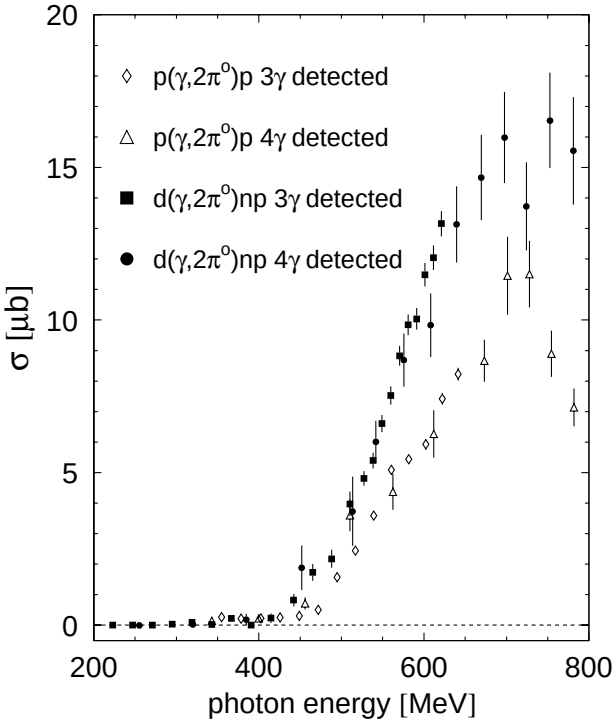

Fig. 14. Total cross section of the reactions $d(\gamma,\pi^o)np$ (filled symbols) and $p(\gamma,\pi^o)p$ [30] (open symbols) (see text).

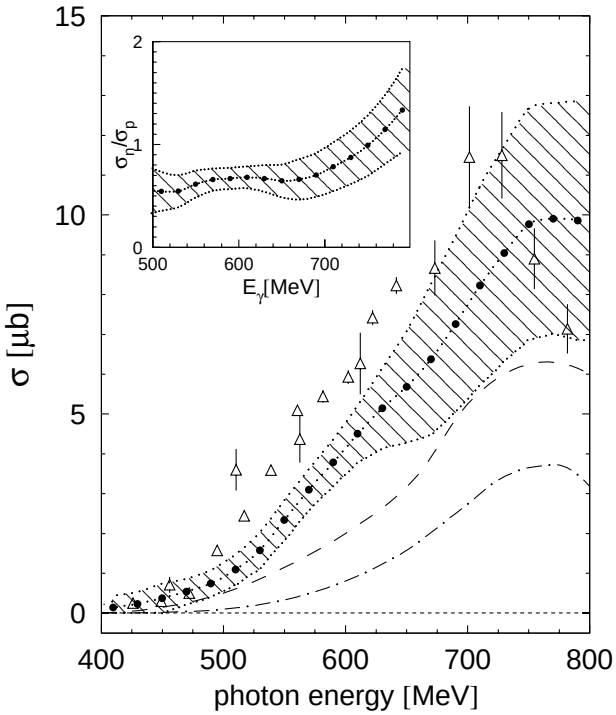

Fig. 15. Total cross section of the reaction $n(\gamma,2\pi^o)n$. The dots correspond to the cross section deduced from the measured values for the proton and deuteron target in a participant – spectator approximation taking into account effects of Fermi smearing. The hatched area symbolises the uncertainty of this result. The dashed and dash-dotted lines are the model predictions from Gomez-Tejedor et al. [14] and Ochi et al. [15], respectively. The cross section for the $p(\gamma,2\pi^o)p$-reaction (open triangles) is shown for comparison. The insert shows our estimate for the ratio of neutron and proton cross section.

First attempts of measuring double π^o-photoproduction from nuclei have been undertaken. The results will be reported elsewhere. However the interpretation of the nuclear data requires knowledge about the neutron cross section. Up to now double π^o-photoproduction from the deuteron has not been measured. In the present experiment the reaction $d(\gamma,\pi^o\pi^o)np$ was identified with the methods discussed in Sect. 3.2. The total cross section is compared to the proton data [30] in Fig. 14.

An estimate of the cross section of the $n(\gamma,2\pi^o)n$ reaction was extracted from the data in a participant – spectator approach as discussed for η-photoproduction in [4]. The cross section of the $p(\gamma,2\pi^o)p$ reaction and an ansatz for the $n(\gamma,2\pi^o)n$ cross section were folded with the momentum distribution of the bound nucleons taken from the deuteron wave function [33]. The neutron cross section was varied until the sum of proton and neutron cross sections reproduced the measured $d(\gamma,2\pi^o)np$ cross section. Deuteron effects beyond Fermi smearing are not included in this analysis. The justification of this approximation comes from the experimental comparison of $\pi^+\pi^-$ photoproduction from the free and bound proton [6] where no medium effects beyond Fermi smearing have been observed. We therefore can safely assume that nuclear effects like FSI are not important for double pion production in this energy range.

The result of this analysis is compared to model predictions in Fig. 15. The calculations by Gomez-Tejedor et al. [14] and Ochi et al. [15] are somewhat lower than the experimental result, which is more comparable to the $p(\gamma,2\pi^o)p$ cross section also shown in the figure. However, the uncertainty of the data is still quite large.

4.4 Inclusive π^o-photoproduction

The results for the $d(\gamma,\pi^o)np$, $d(\gamma,\pi^o)d$, and $d(\gamma,2\pi^o)np$ reactions reported here together with the cross sections for $d(\gamma,\eta)np$ from [4] and $d(\gamma,\pi^o\pi^-)pp$ from [6] imply that in the energy range up to 800 MeV all reactions on the deuteron with a neutral pion in the final state with the exception of the $d(\gamma,\pi^o\pi^+)nn$ reaction have been directly measured. The total cross section data from the present work is summarized in Tables. 1, 2.

The work of Zabrodin et al. [6] has shown that the quasifree $d(\gamma,\pi^o\pi^-)pp$ cross section and the $p(\gamma,\pi^o\pi^+)n$ cross section are very similar. They differ only in the same way as $\pi^+\pi^-$-photoproduction from the free and bound proton which show no deuteron effects beyond Fermi smearing. We can thus assume that the cross section of the $d(\gamma,\pi^o\pi^-)pp$ and $d(\gamma,\pi^o\pi^+)nn$ reactions are very similar. Under this assumption we can calculate the inclusive π^o-photoproduction cross section from the deuteron by summing up all partial channels properly weighted with

Table 1. Total π^o-photoproduction from the deuteron. The reaction $d(\gamma,\pi^o x)X$ includes multiple pion production, $d(\gamma,\pi^o)X$ stands for the sum of incoherent and coherent single π^o-photoproduction. The errors are statistical (errors in brackets: systematic uncertainty of the coherent – incoherent separation). The additional overall normalization error is 6%.

E_γ	$\sigma_t[\mu b]$			
MeV	$d(\gamma,\pi^o x)X$	$d(\gamma,\pi^o)X$	$d(\gamma,\pi^o)np$	$d(\gamma,\pi^o)d$
204	59 ± 2	59 ± 1	16 ± 1(2)	43 ± 1(2)
213	75 ± 2	76 ± 2	21 ± 1(3)	55 ± 2(3)
223	103 ± 2	101 ± 2	34 ± 1(3)	68 ± 2(3)
232	130 ± 2	129 ± 2	45 ± 2(4)	84 ± 2(4)
242	163 ± 3	161 ± 3	64 ± 2(5)	97 ± 2(5)
252	198 ± 3	197 ± 3	81 ± 2(7)	117 ± 2(7)
261	239 ± 3	239 ± 3	111 ± 3(8)	129 ± 2(8)
271	284 ± 4	284 ± 4	147 ±3(10)	138 ±2(10)
281	341 ± 4	341 ± 4	193 ±4(12)	148 ±3(12)
290	377 ± 5	378 ± 5	225 ±4(13)	153 ±3(13)
300	426 ± 5	426 ± 5	276 ±5(15)	150 ±3(15)
309	454 ± 5	456 ± 5	315 ±5(16)	141 ±3(16)
319	469 ± 5	472 ± 6	348 ±6(17)	124 ±3(17)
329	485 ± 5	486 ± 6	361 ±6(17)	125 ±2(17)
338	461 ± 5	462 ± 5	353 ±6(17)	109 ±2(17)
348	448 ± 5	450 ± 5	344 ±5(16)	107 ±3(16)
357	430 ± 5	430 ± 5	343 ±5(15)	87 ±2(15)
367	393 ± 5	392 ± 5	318 ±5(14)	74 ±2(14)
376	366 ± 5	364 ± 5	293 ±5(13)	71 ±2(13)
386	342 ± 5	340 ± 5	289 ±5(12)	51 ±2(12)
395	313 ± 5	308 ± 5	254 ±5(11)	53 ±2(11)
405	290 ± 5	283 ± 5	238 ±4(10)	45 ±2(10)
414	263 ± 5	254 ± 5	218 ± 4(9)	37 ± 2(9)
424	252 ± 4	236 ± 3	198 ± 4(8)	39 ± 2(8)
433	225 ± 4	214 ± 4	184 ± 4(8)	29 ± 1(8)
442	206 ± 4	191 ± 4	167 ± 4(7)	23 ± 1(7)
451	190 ± 4	172 ± 4	154 ± 4(6)	18 ± 1(6)
461	180 ± 4	161 ± 4	147 ± 3(6)	14 ± 1(6)
470	171 ± 4	155 ± 4	133 ± 4(5)	22 ± 1(5)
479	162 ± 4	138 ± 3	123 ± 3(5)	15 ± 1(5)
488	151 ± 4	131 ± 4	121 ± 3(4)	11 ± 1(4)
497	147 ± 4	119 ± 3	111 ± 3(4)	8 ± 1(4)
506	140 ± 4	109 ± 3	98 ± 3(4)	11 ± 1(4)
515	139 ± 4	106 ± 5	96 ± 3(4)	10 ± 1(4)
524	128 ± 4	91 ± 1	82 ± 1(3)	10 ± 1(3)
533	135 ± 4	87 ± 1	75 ± 1(3)	12 ± 1(3)
541	127 ± 4	80 ± 1	77 ± 1(3)	2 ± 1(3)
550	125 ± 4	79 ± 1	71 ± 1(3)	7 ± 1(3)
559	132 ± 4	74 ± 1	70 ± 1(2)	4 ± 1(2)
567	120 ± 4	68 ± 1	65 ± 1(2)	3 ± 1(2)
575	129 ± 5	64 ± 1	62 ± 1(2)	2 ± 1(2)
584	121 ± 4	60 ± 1	56 ± 1(2)	3 ± 1(2)
592	129 ± 5	58 ± 1	55 ± 1(2)	3 ± 1(2)
600	124 ± 5	56 ± 1	56 ± 1(1)	1 ± 1(1)
608	128 ± 4	54 ± 1	–	–
616	121 ± 4	51 ± 1	–	–
624	129 ± 5	50 ± 1	–	–
632	132 ± 5	49 ± 1	–	–
640	134 ± 5	46 ± 1	–	–
647	142 ± 5	47 ± 1	–	–
655	138 ± 5	46 ± 1	–	–
662	154 ± 6	45 ± 1	–	–
670	149 ± 6	46 ± 1	–	–

Table 1. (continued) Total π^o-photoproduction cross sections from the deuteron.

E_γ[MeV]	$\sigma_t[\mu b]$			
	$d(\gamma,\pi^o x)X$	$d(\gamma,\pi^o)X$	$d(\gamma,\pi^o)np$	$d(\gamma,\pi^o)d$
677	150 ± 5	47 ± 1	–	–
684	157 ± 6	46 ± 1	–	–
691	166 ± 7	47 ± 1	–	–
698	167 ± 6	48 ± 1	–	–
705	183 ± 7	50 ± 1	–	–
712	177 ± 6	51 ± 1	–	–
718	185 ± 7	49 ± 1	–	–
725	192 ± 7	54 ± 2	–	–
731	198 ± 7	51 ± 2	–	–
738	198 ± 7	52 ± 2	–	–
744	203 ± 7	55 ± 2	–	–
751	215 ± 7	57 ± 1	–	–
758	208 ± 7	52 ± 2	–	–
765	200 ± 7	54 ± 2	–	–
773	218 ± 8	53 ± 2	–	–
779	212 ± 8	50 ± 2	–	–
785	214 ± 8	49 ± 2	–	–
790	215 ± 9	52 ± 2	–	–

Table 2. Total $2\pi^o$-photoproduction cross section from the deuteron. The additional overall normalization error is 10%.

E_γ[MeV]	$\sigma_t[\mu b]$ $d(\gamma,2\pi^o)np$	
	3γ-events	4γ-events
319	0.10 ± 0.05	–
320	–	0.02 ± 0.06
343	0.02 ± 0.07	–
367	0.23 ± 0.10	–
385	–	0.19 ± 0.19
391	0.01 ± 0.10	–
415	0.23 ± 0.15	–
442	0.8 ± 0.2	–
452	–	1.9 ± 0.7
465	1.7 ± 0.3	–
488	2.2 ± 0.3	–
511	4.0 ± 0.4	–
514	–	3.7 ± 1.1
527	4.8 ± 0.3	–
539	5.4 ± 0.3	–
542	–	6.0 ± 0.7
549	6.6 ± 0.3	–
560	7.5 ± 0.3	–
571	8.8 ± 0.3	–
576	–	8.7 ± 0.9
581	9.8 ± 0.4	–
591	10.0 ± 0.4	–
601	11.5 ± 0.4	–
608	–	9.8 ± 1.0
611	12.0 ± 0.4	–
621	13.2 ± 0.4	–
640	–	13.1 ± 1.3
669	–	14.7 ± 1.4
698	–	16.0 ± 1.5
724	–	13.7 ± 1.5
753	–	16.5 ± 1.6
781	–	15.6 ± 1.8

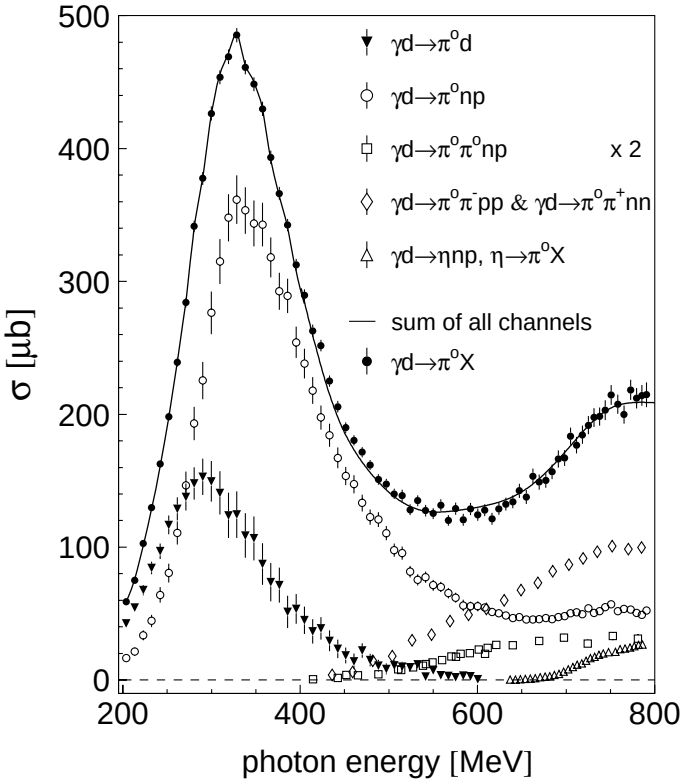

Fig. 16. Neutral pion photoproduction from the deuteron. The cross section for the final states $\pi^o\pi^- pp$ and $\pi^o\pi^+ nn$ was deduced from the DAPHNE data [41,6], the cross sections for π^o from η-decays are taken from ref [44]. The full line represents the sum of all exclusive channels and agrees very well with the measured inclusive cross section.

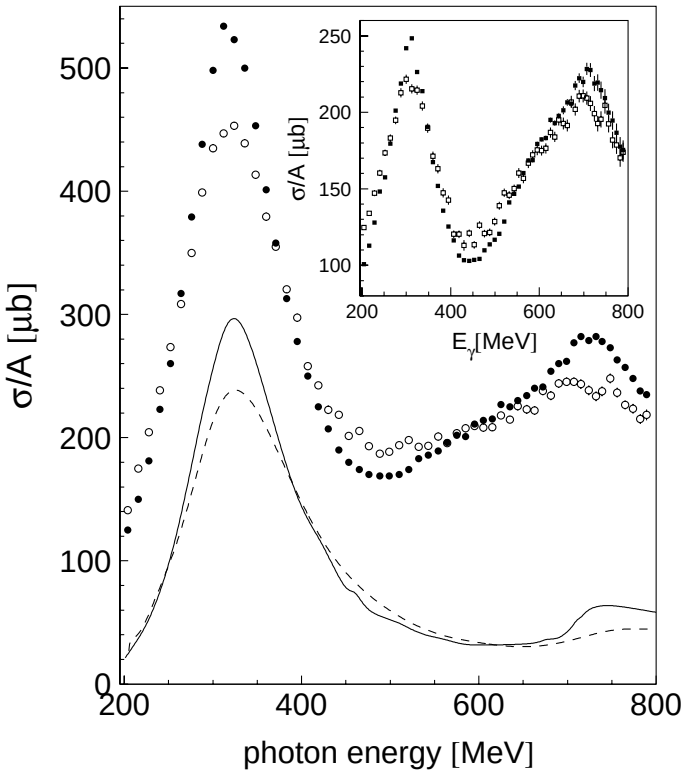

Fig. 17. Comparison to total photoabsorption data. The total photoabsorption cross section per nucleon from the proton [35] (full circles) and the deuteron [35] are compared to the cross sections involving neutral meson production (π^o, $2\pi^o$, η) (proton: solid curve, deuteron: dashed curve). The insert shows the difference of total photoabsorption and neutral meson production (proton: filled squares, deuteron: open squares)

the neutral pion multiplicity and in case of the η-decays into three pions weighted with the branching ratios.

The result is shown in Fig. 16. The full line corresponds to the sum of all partial channels. On the other hand, we have directly measured inclusive π^o-production from the deuteron by analysing all events with at least one π^o in the final state. This result is also shown in Fig. 16 and agrees very well with the summed up partial cross sections. The agreement suggests that systematic uncertainties of the partial cross sections, which all involve complicated analyses and have been measured with two different detector systems (TAPS [27] and DAPHNE [49]), are very well under control and that the contribution of triple pion production apart from the η-decays is negligible.

The contribution of reactions involving only neutral meson production (π^o, $2\pi^o$, η) to the total photoabsorption cross section can be determined by summing up the partial cross sections without weighting them by their π^o-multiplicities. The cross section for the proton was obtained by summing up the partial channels from [1,30, 32]. The results are compared in Fig. 17 to the total photoabsorption data from [35].

It is obvious from the comparison that most of the discrepancy between proton and deuteron cross section per nucleon comes from the neutral channels. The difference between total photoabsorption and the cross section for the neutral channels, which represents the sum of the $\pi^{\pm}$, $\pi^+\pi^-$ and $\pi^o\pi^{\pm}$ cross sections, is very similar for proton und deuteron (see insert of Fig. 17). Consequently the ratio of the cross section sum of $p(\gamma,\pi^+)n$, $p(\gamma,\pi^o\pi^+)n$, $p(\gamma,\pi^+\pi^-)p$ to the cross section of $n(\gamma,\pi^-)p$, $n(\gamma,\pi^o\pi^-)p$, $n(\gamma,\pi^+\pi^-)n$ must be close to unity throughout the first and second resonance regions.

5 Summary and conclusions

Total and differential cross sections have been measured for the $d(\gamma,\pi^o)d$, $d(\gamma,\pi^o)np$, $d(\gamma,2\pi^o)np$ and $d(\gamma,\pi^o)X$ reactions in the energy range from 200 to 800 MeV covering a large angular range. It was demonstrated that the data for the different partial reaction channels add up together with the data for $\pi^+\pi^o$- and $\pi^-\pi^o$-photoproduction measured with the DAPHNE-detector [41,6] to the total inclusive π^o-photoproduction cross section from the deuteron. This demonstrates the good control of systematical uncertainties. The comprehensive data set allows stringent tests of existing model predictions.

In the energy range of the Δ-resonance we find good agreement with model predictions [10,8,7,9,11] for coherent π^o-photoproduction. There is some indication for the

presence of final state interaction effects since their inclusion improves the agreement between data and calculations. However, the effects are not very large and different models do not agree about the main FSI mechanisms. Kamalov et al. [10] have argued that the main effect comes from elastic pion rescattering, while Wilhelm et al. [11] in their model find important contributions from charge exchange scattering. Their predictions for FSI effects disagree even qualitatively. The data are somewhat better reproduced by the prediction from [10], but the two models follow very different lines not only for the FSI effects. Their predictions without FSI effects are at least as different as the full calculations so that no final conclusion about FSI mechanisms can be reached.

Final state interaction is a much more important effect for the $d(\gamma,\pi^o)np$ breakup reaction. The comparison of the data to models [8,12] demonstrates the large influence of np-rescattering. The prediction [8,13] was, that the cross section at pion forward angles, where the relative energy of the np-pair is comparatively low, will be much smaller than expected in a simple participant-spectator approximation. This effect is clearly visible in the data, which at forward angles are in quite good agreement with the prediction from [8]. The data are somewhat lower than the prediction at backward angles which might indicate that some effects are still missing in the model. Interestingly, in spite of the presence of the FSI effects, the angular distributions close to the Δ-peak position exhibit the characteristic shape expected for the excitation of the Δ via the dominant M_{1+}-multipole. However, it is evident that any attempts of extracting the $n(\gamma,\pi^o)n$ cross section in the Δ-resonance region from the breakup reaction, which would be very interesting for the isospin separation of the multipoles, requires careful consideration of the FSI effects. On the experimental side the situation may be improved by coincident detection of the recoil nucleons. This will allow to reduce the importance of FSI effects by selecting events where the neutron exhibits quasifree kinematics.

In the intermediate energy range for incident photon energies between 500 and 650 MeV the breakup cross section per nucleon is very similar to π^o-production from the proton. However, in the second resonance region, at energies between 650 and 800 MeV, the structure in the $p(\gamma,\pi^o)p$ cross section is almost completely suppressed in the deuteron data. The interpretation of this effect requires a more detailed study of the contribution from resonance excitations and the η-cusp effect to the elementary reaction on the proton.

Finally, quasifree double π^o-photoproduction from the deuteron was measured for the first time and used to approximate the neutron cross section, which seems to be comparable to the proton cross section.

We wish to acknowledge the excellent support of the accelerator group of MAMI, as well as many other scientists and technicians of the Institut für Kernphysik at the University of Mainz. We are very grateful to H. Arenhövel, J.M. Laget, S.S. Kamalov, R. Schmidt, and L. Tiator who provided us with the results of their models. This work was supported by Deutsche Forschungsgemeinschaft (SFB 201) and Bundesministerium für Bildung und Forschung (BMBF, Contract No. 06 GI 475(3)I).

References

1. B.Krusche et al., Phys. Rev. Lett. **74**, 3736 (1995)
2. B.Krusche et al., Phys. Lett. **B397**, 171 (1997)
3. P.Benz et al., Nucl. Phys. **B65**, 158 (1973)
4. B.Krusche et al., Phys. Lett. **B358**, 40 (1995)
5. P.Hoffmann-Rothe et al., Phys. Rev. Lett. **78**, 4697 (1997)
6. A.Zabrodin et al., Phys. Rev. **C55**, R1617 (1997)
7. F.Blaazer et al., Nucl. Phys. **A590**, 750 (1995)
8. J.M.Laget, Phys. Rep. **69**, 1 (1981), and private communication
9. P.Bosted and J.M.Laget Nucl. Phys. **A296**, 413 (1978)
10. S.S.Kamalov, L.Tiator, C.Bennhold, Phys. Rev. **C55**, 98 (1997)
11. P.Wilhelm and H. Arenhövel, Nucl. Phys. **A593**, 435 (1995) and **A609**, 469 (1996)
12. R.Schmidt, H.Arenhövel and P.Wilhelm, Z. Phys. **A355**, 421 (1996) and private communication
13. M.I.Levchuk, V.A.Petrun'kin and M.Schumacher, Z. Phys. **A355**, 317 (1996)
14. J.A.Gomez-Tejedor and E.Oset, Nucl. Phys. **A600**, 413 (1996)
15. K.Ochi et al., nucl-th/9703058 (1997); M.Hirata et al., nucl-th/9711031 (1997)
16. E.Hilger et al.,Nucl. Phys. **B93**, 7 (1975)
17. G.von Holtey et al., Z. Phys. **259**, 51 (1973)
18. B.Bouquet et al., Phys. Lett. **B41**, 536 (1972); B.Bouquet et al., Nucl. Phys. **B79**, 45 (1974)
19. A.Imanishi et al., Phys. Rev. Lett. **54**, 2497 (1985)
20. W.Beulertz, Ph.D. thesis, Universität Bonn, 1994
21. J.C.Bergstrom et al., Phys. Rev. **C57**, 3203 (1998)
22. R.W.Clift et al., Phys. Rev. Lett. **33**, 1500 (1974)
23. C.Bacci et al., Phys. Lett. **B39**, 559 (1972)
24. Y. Hemmi et al., Phys. Lett **B32**, 137 (1970); Y. Hemmi et al., Nucl. Phys. **B55**, 333 (1975)
25. Th.Walcher, Prog. Part. Nucl. Phys. **24**, 189 (1990)
26. I.Anthony et al., Nucl. Inst. Meth. **A301**, 230 (1991)
27. R.Novotny, IEEE Trans. Nucl. Scie. **38**, 379 (1991)
28. A.R.Gabler et al., Nucl. Instr. and Meth. **A346**, 168 (1994)
29. R.Brun et al., GEANT, Cern/DD/ee/84-1, 1986
30. F.Härter et al., Phys. Lett. **B401**, 229 (1997)
31. M.Fuchs et al., Phys. Lett. **B368**, 20, (1996); M.Fuchs, PhD thesis, University of Giessen (1995), unpublished
32. F.Härter, PhD thesis, University of Mainz (1996) KPH15/96, unpublished
33. M.Lacombe et al., Phys. Lett **B101**, 139 (1981)
34. T.A.Armstrong et al., Phys. Rev. **D5**, 1640 (1972); T.A.Armstrong et al., Nucl. Phys. **B41**, 445 (1972)
35. M.MacCormick et al., Phys. Rev. **C53**, 41 (1996)
36. R.Arndt et al., VPI and SU Scattering Analysis Interactive Dialin
37. K.H.Althoff et al., Z. Phys. **C1**, 327 (1979)
38. I. Strakovsky, private communication
39. R.Beck et al., Phys. Rev. Lett. **78**, 606 (1997)

40. O.Hanstein et al., Nucl Phys. **A632**, 561 (1998)
41. A.Braghieri et al., Phys. Lett. **B363**, 46 (1995)
42. L.Y.Murphy and J.M.Laget, DAPHNIA/SPhN **96-10**, (1996)
43. N.Bianchi et al., Phys. Lett. **B299**, 219 (1993)
44. M.Röbig-Landau et al., Phys. Lett. **B373**, 45 (1996)
45. C.Caso et al., *(Review of Particle Physics)* European Phys. J. **C3**, 1 (1998)
46. N.Kaiser et al., Nucl. Phys. **A612**, 297 (1997)
47. T.Waas and W.Weise, Nucl. Phys. **A625**, 287 (1997)
48. M.Hirata et al., Phys. Rev. Lett. **80**, 5068 (1998)
49. G.Audit et al., Nucl. Instr. and Meth. **A301**, 473 (1991)